

Update on the 3D Kaon Imaging analyses

Róbert Vértési, Michal Šumbera, Petr Chaloupka

Řež/Prague, February 2, 2013

Abstract

This note is an addendum to the $\sqrt{s_{NN}}=200$ GeV Run4+Run7 and Run4 m_T -dependent kaon imaging analyses [1, 2]. The consistency and systematics of the fit parameters are addressed in this note. Different trial functions are employed in order to get a more realistic error estimate of the source. An upper limit on the effect of the feed-down from $\phi(1020)$ mesons on the strength of the K^-K^- Bose-Einstein Correlations is estimated using simulations based on the core-halo picture.

1 Systematics on the fit parameters

The correlation momenta (C_0, C_{x2} etc.) are only slightly effected by PID cuts and track momentum effects, and the different setups yield results which are consistent with each other within their statistical errors. However, due to the sensitive fitting algorithm this is not the case for the fit parameters R_x, R_y, R_z and especially λ . Since the systematics are driven by the statistical variation of the correlation momenta, there are some things to note:

- A systematic variation of the above effects cause these parameters to move within a certain range, basically regardless of the variation itself. Adding up errors quadratically as if they were independent and poisson-distributed would be an overestimation. One can estimate the instability of the parameters by taking the maximum variation instead. Although the primer cause is systematics, the effect is amplified by a process sensitive to pure statistics, and it will be the dominant error over the statistical error of *a particular* fit. Both are shown but the latter is barely visible in the majority of cases.
- It also means that there may be systematic errors that show up uniformly in all setups and do not cause a change in the parameters. For instance if there is a contamination of the kaon sample that cannot be get rid of by applying stricter purity cuts, it will be shown up as a decreased λ parameter but will not show up in the error. Our errors only account for the *uncertainty* and not the *shift*.

The PID was varied between $-0.5 < \sigma_K < 2.0$ and $-1.5 < \sigma_K < 2.0$ in order to estimate the maximum effect. Momentum resolution was smeared by 20%. Notes: 1) PID uncertainty in the lower k_T bin was estimated from the representative relative uncertainty of Run4 data to be 8%. 2) We expect momentum variation to cause an effect effect in

the high- k_T bin that is lower than the PID effect. The fit parameters with statistical and systematic errors finally taken into account are listed in table 1. The fit parameters are summarized in Fig. 1

Cent.	k_T [MeV]	$\sigma_{K,\text{smear}}$	λ	R_x [fm]	R_y [fm]	R_z [fm]	χ^2/ndf
0–20%	200..360	-1.5..2.0	0.485 ± 0.013	4.76 ± 0.07	4.32 ± 0.06	4.72 ± 0.08	497/289
		-2.0..2.0	0.417	4.60	4.28	4.55	
		unsmear	0.467	5.00	4.28	4.83	
0–30%	200..360	-1.5..2.0	0.393 ± 0.013	4.34 ± 0.13	4.00 ± 0.11	4.33 ± 0.17	316/283
		-0.5..2.0	0.484	4.76	4.32	4.72	
		unsmear	0.305	3.91	3.92	4.09	
0–30%	360..480	-1.5..2.0	0.270 ± 0.013	4.46 ± 0.11	3.72 ± 0.09	3.57 ± 0.12	367/283
		-0.5..2.0	0.265	4.76	3.61	3.30	
		-1.0..2.0	0.274	4.46	3.72	3.57	
		-2.0..2.0	0.238	4.24	3.74	3.50	
		unsmear	0.246	4.47	3.55	4.40	

Table 1: Systematic fits. Lines with bold values are the default scenarios, with statistical (fit) errors on parameters and χ^2/ndf values specified. Other lines are systematic variations.

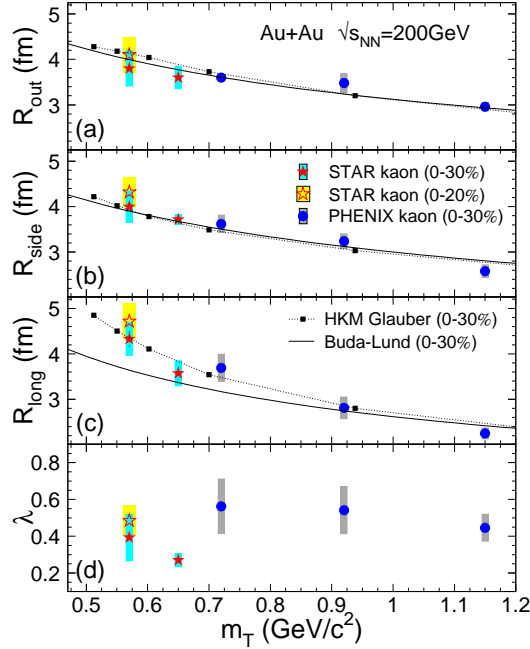


Figure 1: Updated errors on fitted radii and λ vs. transverse mass.

2 Different trial functions

The 3D Gaussian test function for the source describes the correlation moments within errors without a doubt, with a $\chi^2/ndf = 1.7$. However, the latter errors are large enough allow for a non-negligible deviation, and such a trend can be seen in the second moment in the side direction. We tested the fit with a different function shape, a double 3D Gaussian with 6 parameters. Also the description of the trend is better, the fit is not good and due to the large number of parameters it is underdetermined. See Fig. 2. The parameters are $\lambda = 0.483 \pm 0.013$, $R_{x1} = 4.67 \pm 0.07$, $R_{y1} = 4.41 \pm 0.07$, $R_{z1} = 4.62 \pm 0.09$ for the dominant Gaussian (compare it to the 1st line of Table 1), and $\lambda_2 = 0.16 \pm 0.01$, $R_{x2} = 38 \pm 18$, $R_{y2} = 0.61 \pm 0.63$, $R_{z2} = 46 \pm 32$ for the weaker component. The fit has a $\chi^2/ndf = 479/271$. Fits to other datasets are listed in Table 2. Note that that the fit parameters are very firm and insensitive to the shape assumption, but that there is a place for a second component over the Gaussian which only has structure in the side direction (also see the huge values of radii in the out and long direction). The fact that the double Gaussian fit has a similar χ^2/ndf and that the secondary component is undetermined shows that double Gaussian is not a better global shape assumption than simple Gaussian. On the other hand it gives a description that is in point-by-point statistical agreement to the individual moments. Therefore the double Gaussian is a good method to estimate the possible extent of deviation of the source shape from Gaussian (See Fig. 3). In order to draw an upper limit on $\lambda_2 S(r_{x,y,z})$ one can push the fit parameters to the edge of their error range by hand, as shown on Figs. 4 and 5. However, this is a vast overestimation and therefore not used when determining the final errors.

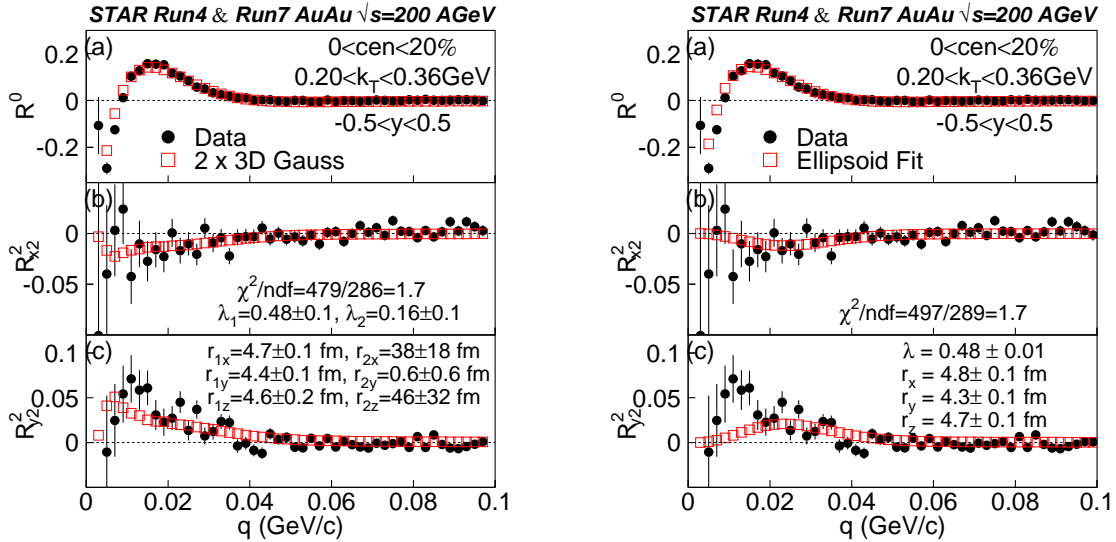


Figure 2: Fit with two 3D Gaussians on top of each other (left) compared to one 3D Gaussian (right).

Cent.	k_T [MeV]	#gaus	λ	R_x [fm]	R_y [fm]	R_z [fm]	χ^2/ndf
0–20%	200..360	1st	0.483 ± 0.013	4.67 ± 0.07	-4.41 ± 0.07	4.62 ± 0.09	479/286
		2nd	0.16 ± 0.10	38 ± 18	0.61 ± 0.63	46 ± 32	
0–30%	200..360	1st	0.383 ± 0.022	4.21 ± 0.14	4.20 ± 0.13	4.16 ± 0.17	307/286
		2nd	0.05 ± 0.03	12 ± 5	0.2 ± 0.5	14 ± 8	
0–30%	360..480	1st	0.270 ± 0.013	4.46 ± 0.11	3.72 ± 0.09	3.57 ± 0.12	367/286
		2nd	0.61 ± 0.65	27 ± 5	15 ± 5	30 ± 5	

Table 2: Double Gaussian fit parameters.

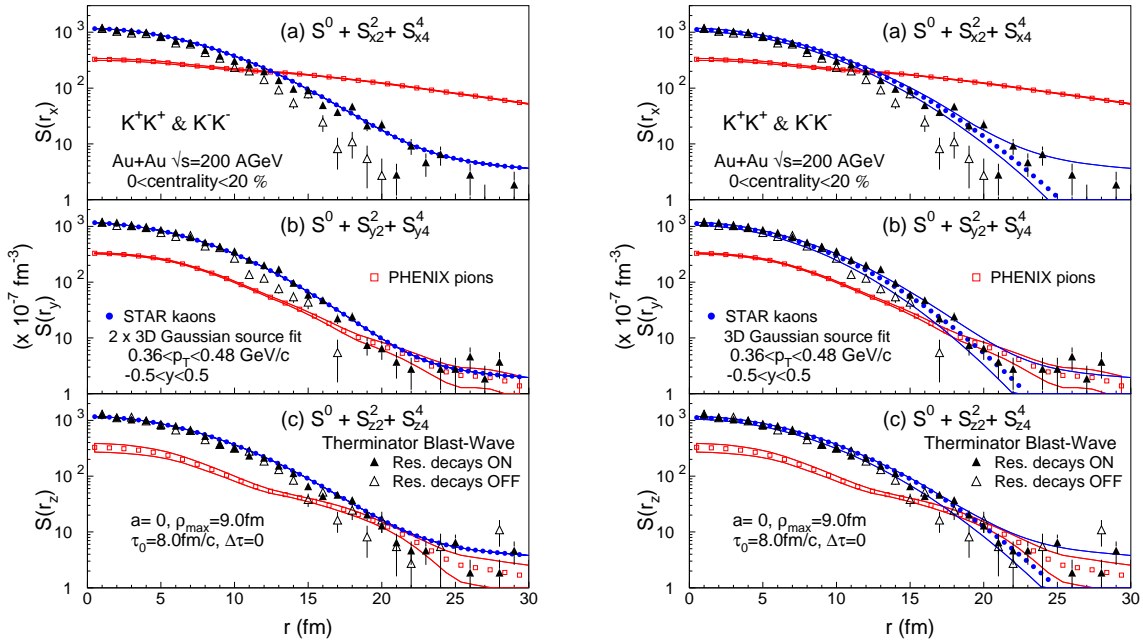


Figure 3: *Left*: Source from double Gaussian fit (no error range shown.). *Right*: STAR $S(r_{x,y,z})$ with errors including shape assumption.

3 Estimated fit stability from the tails of C_0

Because of the sensitiveness of the fit process a question arises how stable the obtained fit parameters are, i.e. are the values and systematics in the range we claim. The most sensitive is λ , being responsible to the absolute normalization. We present an additional check here where the tails of the $C_0(q)$ distributions are fitted. Since all the effects present at small q are neglected, one doesn't expect of course the *same* value for λ . What is expected, however, is that λ be in the same ballpark to what is obtained from the simultaneous fit. Furthermore, if this fit is stable, it indicates that λ from the simultaneous fit is less prone to artefact effects from statistics. What we did here was fitting the tails, varying the minimum value (cutoff) for the fit between $0.16 < q < 0.30$ GeV/c. See Figs. 6, 7 and 8 for the results. It is to be concluded that

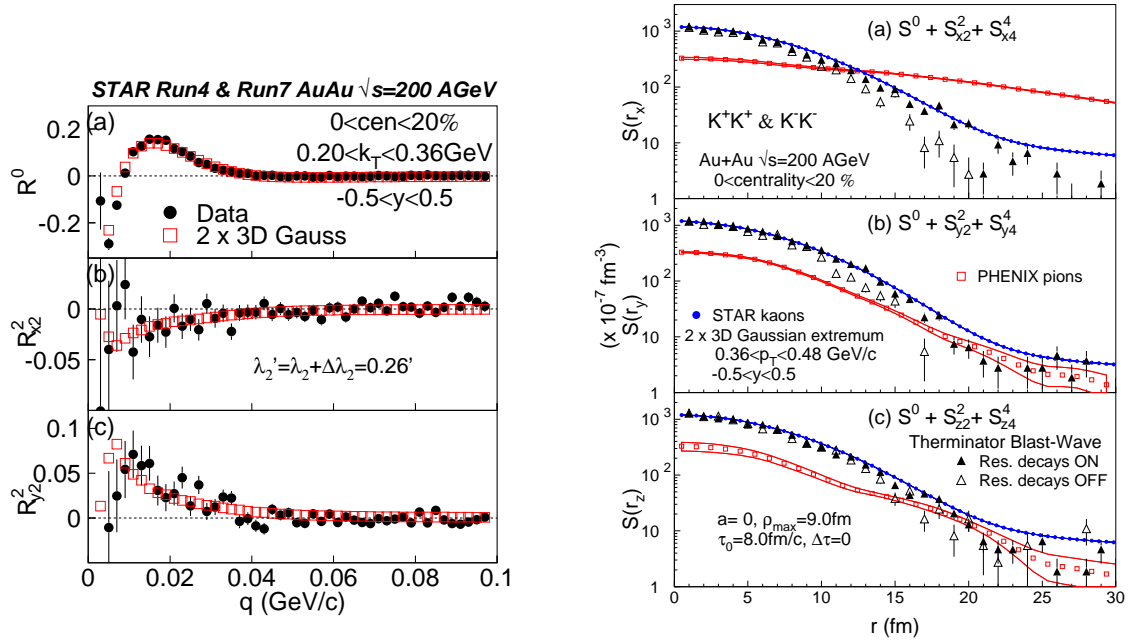


Figure 4: Double Gaussian correlation moment fit (*left*) and reconstructed source (*right*) with the height of secondary gaussian maxed out ($\lambda_2 = 0.26$, no fit error range shown).

1) λ obtained from the tail fits is similar in height to those from the simultaneous fits (although there is a 30% difference in the high- k_T bin due to the much more pronounced role of higher momenta), and 2) that tail λ fits in the higher k_T bin is much more stable, much more confined by a single momentum, in accordance with the sizes of systematic errors on the simultaneous fits.

4 Effect of the feed-down from ϕ mesons

Besides kaon purity, a general shift in λ can be caused by long lived resonance. In the core-halo picture [3, 4, 5] the correlation function can be expressed with the extrapolated intercept parameter λ_* as

$$C(\Delta k, K) = 1 + \lambda_* R_c, \quad (1)$$

where R_c is defined by the Fourier transform of the one particle emission function $S_c(x, K)$ of the core as

$$R_c = \frac{|\tilde{S}_c(\Delta k, K)|^2}{|\tilde{S}_c(0, K)|^2},$$

$$\tilde{S}_c(\Delta k, K) = \int d^4x S_c(x, K) e^{i\Delta k x}, \quad (2)$$

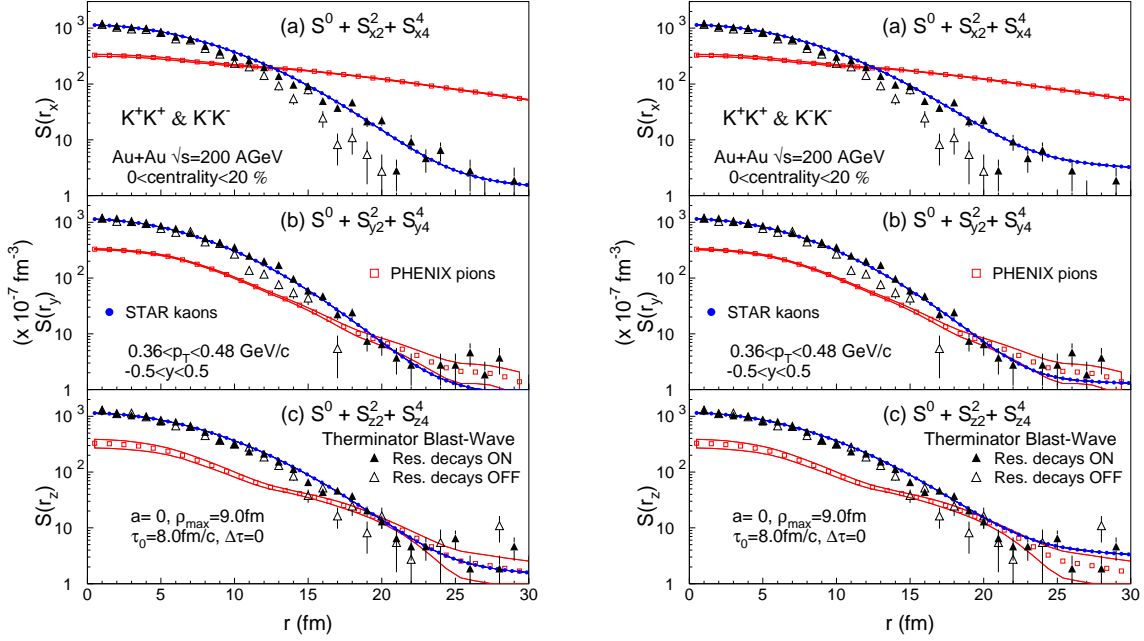


Figure 5: *Left*: Double Gaussian reconstructed source with secondary out and long radii at maximum ($R_{2o} = 56$ fm, $R_{2l} = 78$ fm, no fit error range shown). *Right*: Secondary side radii at maximum ($R_{2s} = 1.3$ fm).

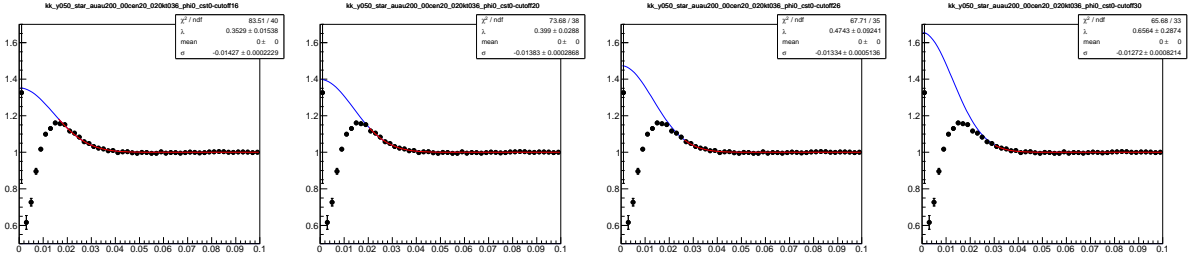


Figure 6: Cutoff fits, Run4+Run7 data, cent<20%, low k_T . Variation of cutoff between $0.16 < q < 0.30$ GeV/c causes λ to ...

and the intercept parameter λ_* is derived from the extrapolation of the correlation value to $\Delta k = 0$, as $\lambda_* = C(0, K) - 1$. (Note that $\lambda_* \equiv \lambda$ if the source is Gaussian.) However, this extrapolation does not include the correlation between halo-halo and core-halo particle pairs, supposed to be unresolvable by our detectors. The intercept parameter can also be expressed directly with the fraction of the core kaons to the total number of kaons:

$$\lambda_*(m_T) = \left(\frac{N_{core}(m_T)}{N_{core}(m_T) + N_{halo}(m_T)} \right)^2. \quad (3)$$

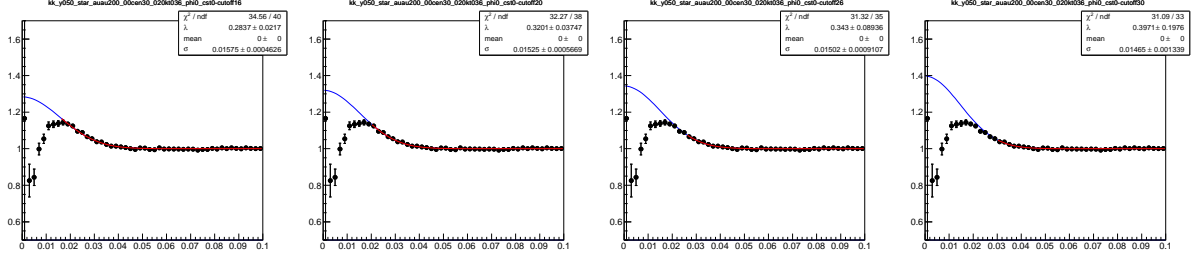


Figure 7: Cutoff fits, Run4 data, cent < 30%, low k_T .

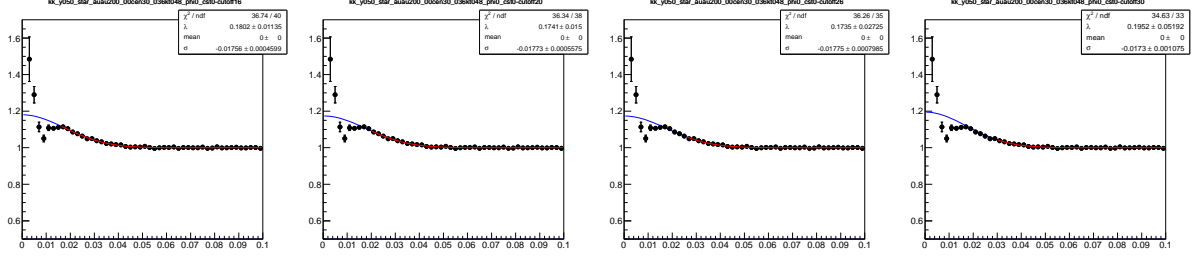


Figure 8: Cutoff fits, Run4 data, cent < 30%, high k_T .

The core in our case consists of kaons emerging immediately after the freezeout including not only primordial particles, but decay kaons of fast-decaying resonances such as K^* that are not separable by BEC measurements. The main contributor to the halo is therefore the long-lived $\phi(1020)$ meson, and the number of halo kaons can be approximated as

$$N_{halo}^{K^-}(m_T) = N_{\phi}(m_T) \times BR(\phi \rightarrow K^- K^+) \quad (4)$$

The global number of K^- and ϕ were fixed to each other using the ratio $\phi/K^- = 0.158 \pm 0.030$ measured by the STAR experiment [6]. The errors on the ratio are propagated to the final result.

The spectra of the particles were assumed to follow a radial flow effected Hagedorn formula,

$$N(m_T) = Ae^{-m_T/T_{eff}} \quad (5)$$

where the effective freeze-out temperature T_{eff} is defined as $T_{eff} = T_{FO} + m \langle u_T \rangle^2$. The values of freeze-out temperature T_{FO} and the average radial flow $\langle u_T \rangle$ of slope fits from PHENIX spectra [7] were used. For central collisions $\langle u_T \rangle = 0.48 \pm 0.07$ was used, while for minbias collisions $\langle u_T \rangle = 0.40 \pm 0.07$ was employed. The error on $\langle u_T \rangle$ was propagated to the systematics of the results. The value $T_{FO} = 177.0 \pm 1.2 \text{ MeV}$ is adequate for both cases. (Considering that the two fit parameters are highly correlated and that the relative error on T_{FO} is negligible compared to that on $\langle u_T \rangle$, the former was not considered.) Decays of the ϕ were simulated using JETSET 7.4.

Simulated intercept parameters are shown w.r.t. transverse mass and momentum in Fig. 9 and Fig. 10 respectively, for $\sqrt{s_{NN}} = 200 \text{ GeV}$ in the midrapidity range $|y| < 0.5$, with radial flow values corresponding to both central and minimum bias collisions. The effect of ϕ on the intercept parameter is approximately 20% at low transverse momenta at both $\langle u_T \rangle$ values, while it is moderated to 6–8% at $p_T = 1.2 \text{ GeV}$. The absolute size of the errors from the considered effects is in the range of 3–5% of the λ_* .

Note that this approach is only valid if the decay width to kaons is not altered substantially within the hadronic medium. In a scenario suggested by Ref. [8] the effective width is dominated by the scattering length of ϕ in the kaon rest system, $l_\phi = 11.9$ fm. Therefore the above results are to be taken as an upper limit of the effect of the ϕ meson on the λ_* .

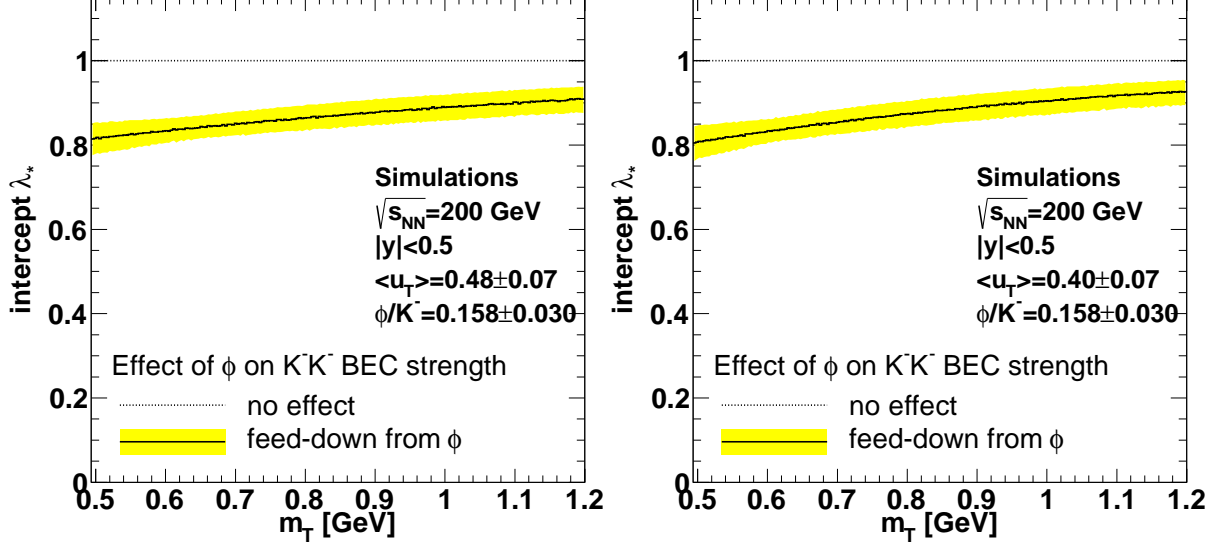


Figure 9: Simulated intercept parameter w.r.t. transverse mass $\lambda_*(m_T)$ in $\langle u_T \rangle = 0.48 \pm 0.07$ corresponding to central collisions (left), and $\langle u_T \rangle = 0.40 \pm 0.07$ corresponding to minimum bias collisions (right). Bands include systematics from both the uncertainties on the ϕ/K^- ratio and on $\langle u_T \rangle$.

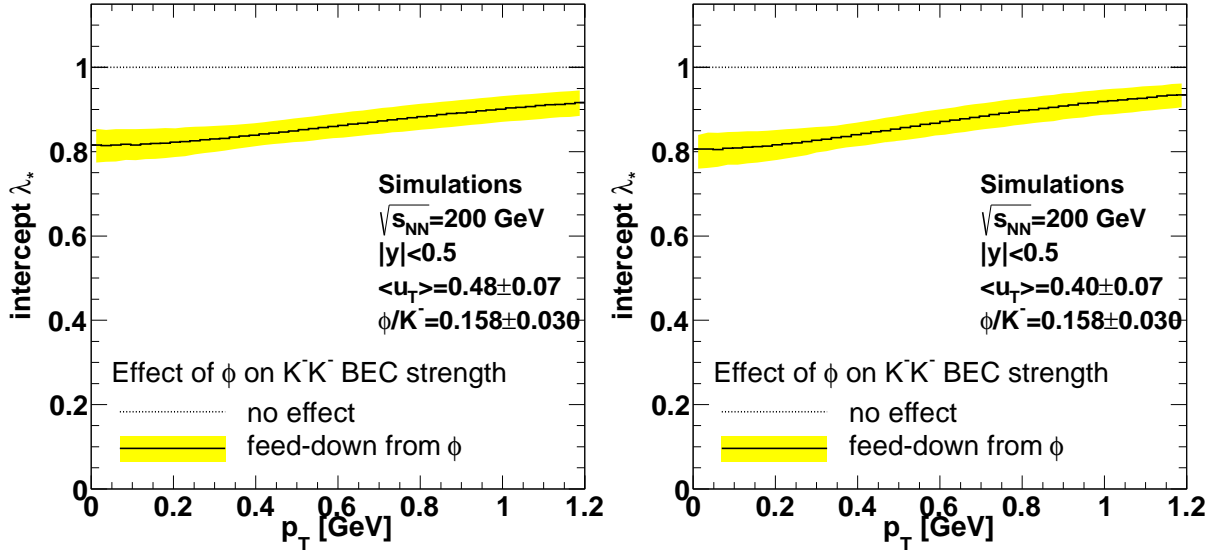


Figure 10: Simulated intercept parameter w.r.t. transverse momentum $\lambda_*(p_T)$ in $\langle u_T \rangle = 0.48 \pm 0.07$ corresponding to central collisions (left), and $\langle u_T \rangle = 0.40 \pm 0.07$ corresponding to minimum bias collisions (right). Bands include systematics from both the uncertainties on the ϕ/K^- ratio and on $\langle u_T \rangle$.

References

- [1] P. Chung, M. Sumbera, P. Chaloupka, J. Kapitan, J. Bielcikova and M. Zerola, "Extraction of Kaon 3D Source Function in 200 GeV Au+Au Collisions at RHIC-STAR", PSN0554, 2011.
- [2] P. Chung, D. Tlusty, J. Kapitan, M. Sumbera, P. Chaloupka, "Kaon Femtoscopy in $\sqrt{s_{NN}}=200$ GeV Au+Au Collisions at RHIC-STAR", http://www.star.bnl.gov/protected/bulkcorr/rvertesi/kaonPaper/Analysis_note.pdf, 2011.
- [3] R. Lednicky and M. I. Podgoretsky, "The Interference Of Identical Particles Emitted By Sources Of Different Sizes," Sov. J. Nucl. Phys. **30**, 432 (1979) [Yad. Fiz. **30**, 837 (1979)].
- [4] T. Csörgő, B. Lörstad and J. Zimányi, "Bose-Einstein correlations for systems with large halo," Z. Phys. C **71**, 491 (1996) [hep-ph/9411307].
- [5] J. Bolz, U. Ornik, M. Plumer, B. R. Schlei and R. M. Weiner, "Interferometry of pions and kaons in high-energy collisions," Phys. Lett. B **300**, 404 (1993).
- [6] J. Adams *et al.* [STAR Collaboration], "phi meson production in Au + Au and p+p collisions at $s(NN)^{1/2} = 200$ -GeV," Phys. Lett. B **612**, 181 (2005) [nucl-ex/0406003].
- [7] S. S. Adler *et al.* [PHENIX Collaboration], "Identified charged particle spectra and yields in Au+Au collisions at $S(NN)^{1/2} = 200$ -GeV," Phys. Rev. C **69**, 034909 (2004) [nucl-ex/0307022].
- [8] R. Lednicky and T. B. Progulova, "Influence of resonances on Bose-Einstein correlations of identical pions," Z. Phys. C **55**, 295 (1992).